

XMM-Newton discovery of a sharp spectral feature at ~ 7 keV in the narrow-line Seyfert 1 galaxy 1H 0707 – 495

Th. Boller,^{1★} A. C. Fabian,² R. Sunyaev,³ J. Trümper,¹ S. Vaughan,² D. R. Ballantyne,² W. N. Brandt,⁴ R. Keil¹ and K. Iwasawa²

¹Max-Planck-Institut für extraterrestrische Physik, Postfach 1603, 85748 Garching, Germany

²Institute of Astronomy, Madingley Road, Cambridge CB3 0HA

³Max-Planck-Institut für Astrophysik, 85748 Garching, Germany

⁴Department of Astronomy and Astrophysics, The Pennsylvania State University, 525 Davey Lab, University Park, PA 16802, USA

Accepted 2001 October 12. Received 2001 October 12; in original form 2001 August 2

ABSTRACT

We report the first detection of a sharp spectral feature in a narrow-line Seyfert 1 galaxy. Using *XMM-Newton* we have observed 1H 0707 – 495 and find a drop in flux by a factor of more than 2 at a rest-frame energy of ~ 7 keV without any detectable narrow Fe K α line emission. The energy of this feature suggests a connection with the neutral iron K photoelectric edge, but the lack of any obvious absorption in the spectrum at lower energies makes the interpretation challenging. We explore two alternative explanations for this unusual spectral feature: (i) partial-covering absorption by clouds of neutral material; and (ii) ionized disc reflection with lines and edges from different ionization stages of iron blurred together by relativistic effects. We note that both models require an iron overabundance to explain the depth of the feature. The X-ray light curve shows strong and rapid variability, changing by a factor of 4 during the observation. The source displays modest spectral variability which is uncorrelated with flux.

Key words: galaxies: active – galaxies: individual: 1H 0707 – 495 – galaxies: Seyfert – X-rays: galaxies.

1 INTRODUCTION

1H 0707 – 495 ($B = 15.7$; $z = 0.0411$) has displayed some of the most rapid X-ray variability observed in a Seyfert galaxy (Turner et al. 1999; Leighly 1999a). Its X-ray spectrum is steep and shows a strong ‘soft excess’ (Vaughan et al. 1999; Leighly 1999b), and its optical spectrum shows narrow H β (FWHM of H β = 1050 km s⁻¹) and strong Fe II emission (Remillard et al. 1986; Leighly 1999b), characteristic of many ultrasoft Seyferts. On the basis of the FWHM of H β , 1H 0707 – 495 is classified as a narrow-line Seyfert 1 (NLS1) galaxy.

Such ultrasoft NLS1s are of particular interest because their extreme properties are most likely produced by an extreme value of an underlying physical parameter (e.g. Pounds, Done & Osborne 1995; Boller, Brandt & Fink 1996; Brandt & Boller 1998; Vaughan et al. 2001). However, with a few exceptions, their timing and spectral properties proved difficult to study in detail with previous X-ray observatories as a result of, e.g., regular light curve interruptions from Earth occultation and limited spectral bandpass.

1H 0707 – 495 was observed as part of a guaranteed time programme to study the timing and spectral properties of the X-ray-brightest and most prominent ultrasoft NLS1s using

XMM-Newton. In this Letter we report the first results from the EPIC data, and in particular the detection of an unusual spectral feature at around 7 keV.

2 OBSERVATION AND DATA REDUCTION

XMM-Newton observed 1H 0707 – 495 on 2000 October 21 during rev. 0159 for a duration of 46 ks, during which all instruments were operating nominally. The EPIC-pn camera was operated in full-frame mode, and the two MOS cameras were in large-window mode; all three cameras used the medium filters. Extraction of science products from the Observation Data Files (ODFs) followed standard procedures using the *XMM-Newton* Science Analysis System version 5.1.0 (SAS¹).

The raw MOS and pn data were processed to produce calibrated event lists. Unwanted hot, dead or flickering pixels were removed, likewise events caused by electronic noise, and event energies were corrected for charge-transfer losses. The latest available calibration files² were used in the processing. Light curves were extracted from these event lists to search for periods of background flaring, and showed the background to be stable throughout the duration of

★E-mail: bol@mpe.mpg.de

¹ See http://xmm.vilspa.esa.es/user/sas_top.html

² <http://xmm.vilspa.esa.es/ccf/>

the observation. The total amount of ‘good’ exposure time selected was 42 688 s for MOS1, 42 692 s for MOS2 and 38 106 s for the pn. [The pn exposure time includes a correction for out-of-time events in full-frame mode (Strüder et al. 2001)].

Source data were extracted from circular regions of radius 60 arcsec for the MOS data, and radius 35 arcsec for the pn. (The smaller extraction region was used in the pn in order to avoid the CCD chip boundary ~ 40 arcsec from the pn aimpoint.) The total number of counts for the pn is 52 377, and for MOS1 and MOS2 14 501 and 14 634, respectively. For the pn camera, both source and background regions were taken from inside the area corresponding to the hole in the pn circuit board. An examination of background images and spectra confirmed that the instrumental fluorescence radiation, especially above 7 keV from Cu and Ni, is not affecting the source or background spectra. There are no signs of pile-up in the source region. Events corresponding to patterns 0–12 were extracted from the MOS data. Patterns 0–4 (single- and double-pixel events only) were used for the pn analysis.

3 SPECTRAL ANALYSIS

The source spectra were grouped such that each spectral bin contains at least 20 counts, and were fitted using the XSPEC 11.0.1 software package (Arnaud 1996). The latest publicly available responses were used.³ The spectra from the three detectors were fitted simultaneously but with the relative normalizations free to vary. The quoted errors on the derived best-fitting model parameters correspond to a 90 per cent confidence level for one interesting parameter (i.e. a $\Delta\chi^2 = 2.7$ criterion) unless otherwise stated. Values of $H_0 = 70 \text{ km s}^{-1} \text{ Mpc}^{-1}$ and $q_0 = 0.5$ are assumed throughout, and fit parameters (specifically edge and line energies) are quoted for the rest frame of the source.

Fig. 1 shows the raw count spectra from the EPIC cameras. The broad-band spectrum is steep. A simple power law fitted across the entire spectrum gives a slope $\Gamma \approx 3.8$, but this fit is dominated by the spectrum below 1 keV where the statistics are best. The most striking spectral feature is the sudden drop by a factor of more than 2 at around 7 keV, visible in both pn and MOS spectra (note that this is a lower limit as the energy resolution of about 180 eV will smear a sharp edge). The width of the feature is not significantly larger than the energy resolution. The response matrices do not introduce any strong features around the observed energy of this feature, nor do the cosmic or instrumental backgrounds. In the 7–10 keV range the source is detected with a significance level of about 20σ , therefore the spectral feature is intrinsic to the source. However, the limited photon statistics above 10 keV do not allow us to constrain the expected recovery of the flux at higher energies.

In the absence of any known systematic effect that could introduce such a feature into the spectrum, the rest of this paper discusses possible physical origins of the feature, assuming it to be intrinsic to the source spectrum. The much higher statistical weight at lower energies (owing to the strong soft excess emission and peak in the EPIC response at ~ 1 keV) meant that fits to the full-band spectra were dominated by the soft emission. In order to concentrate on the feature at 7 keV, the data below 2 keV were ignored in the following analysis.

³ m1_medv9q19t5r5_all_15.rsp and m2_medv9q19t5r5_all_15.rsp for MOS1 and MOS2, respectively and epn_ff20_sdY9_medium.rmf for the pn.

3.1 Absorption by neutral iron?

The most natural interpretation for a drop in the spectrum at just above 7 keV is as an absorption edge from a large column of neutral iron (7.112 keV: Henke, Gullikson & Davis 1993; 7.111 keV: Bearden 1964). The 2–10 keV spectrum (see Fig. 2) can be adequately parametrized ($\chi^2 = 192/182$ dof) using a power law and a deep absorption edge ($\tau = 1.8 \pm 0.3$). While providing an acceptable fit to the data, this model is unsatisfactory for a number of reasons. First, the 2–10 keV power-law slope is unusually flat ($\Gamma = 1.07 \pm 0.09$). Secondly, the steep spectrum below 1 keV suggests that there is little ‘cold’ absorption above that expected from the Galactic column ($N_{\text{H}} = 5.8 \times 10^{20} \text{ cm}^{-2}$: Dickey & Lockman 1990). Indeed, the column of cold iron expected from the depth of the putative edge is $N_{\text{Fe}} \approx 6 \times 10^{19} \text{ cm}^{-2}$ which corresponds to $N_{\text{H}} \approx 2 \times 10^{24} \text{ cm}^{-2}$ for solar abundances. At this column density the spectrum should be dominated by absorption at low energies (L-shell iron and K-shell absorption from lower Z elements), whereas it actually steepens considerably in the soft band. Absorption by ionized material can produce a strong iron K edge without significant soft X-ray absorption, but the energy of the putative edge suggests that the absorber is not strongly ionized. The edge energy at 7.04 ± 0.07 keV is consistent with the neutral iron K-edge energies given in the literature.

The fluorescent yield for iron is close to 0.34 (Bambynek et al. 1972). However, there is no strong, narrow 6.4-keV emission line in the EPIC spectrum; the 90 per cent upper limit on the photon flux in a narrow 6.4-keV line is $8 \times 10^{-7} \text{ photon cm}^{-2} \text{ s}^{-1}$ (corresponding to an equivalent width of ~ 90 eV). The estimated photon flux absorbed by the putative edge is $1.2 \times 10^{-5} \text{ photon cm}^{-2} \text{ s}^{-1}$. For a spherically symmetric distribution of absorbing material one expects a ratio of fluorescence line to Fe K absorbed flux approximately equal to the fluorescent yield, modified by the absorption of the 6.4-keV line (which is about a factor of 2.5 here). The measured ratio (of line/edge flux) is ≈ 0.07 , a factor ≈ 2 smaller than expected for a spherical distribution. This suggests that the column density along the line of sight is higher than the average surrounding the X-ray source. The solid angle subtended by the putative absorber, as seen from the X-ray source, is likely to be $\approx 2\pi sr$ (but see also Section 5).

The following subsections discuss two alternative spectral models: specifically, partial absorption by neutral material and reflection from ionized material.

3.2 Partial-covering model

One possible explanation for the 2–10 keV spectral form of 1H 0707 – 495 is partial covering [i.e. a patchy absorber (Holt et al. 1980)]: the observed spectrum is modified by cold absorption at high energies, while at lower energies a relatively unabsorbed component leaks through. A partial-covering model does provide a good fit to the 2–10 keV spectrum ($\chi^2 = 177/178$ dof), using three absorbed power laws to explain the flat spectrum while the deep iron K edge in the most heavily absorbed component explains the 7-keV feature (see Fig. 2). A narrow 6.4-keV iron line is included in the model although, as noted above, it is only poorly constrained by the data. The best-fitting model parameters are as follows: intrinsic power-law slope $\Gamma = 3.5_{-0.4}^{+1.2}$; line-of-sight column densities (and covering fractions) of $N_{\text{H}} \approx 0$ (0.04), 1.3 (0.12) and 4.6 (0.84) (in units of 10^{22} cm^{-2}); and an iron abundance of about 35. Partial ionization of metals could help, but the sharp spectral edge suggests that iron is not strongly ionized and iron

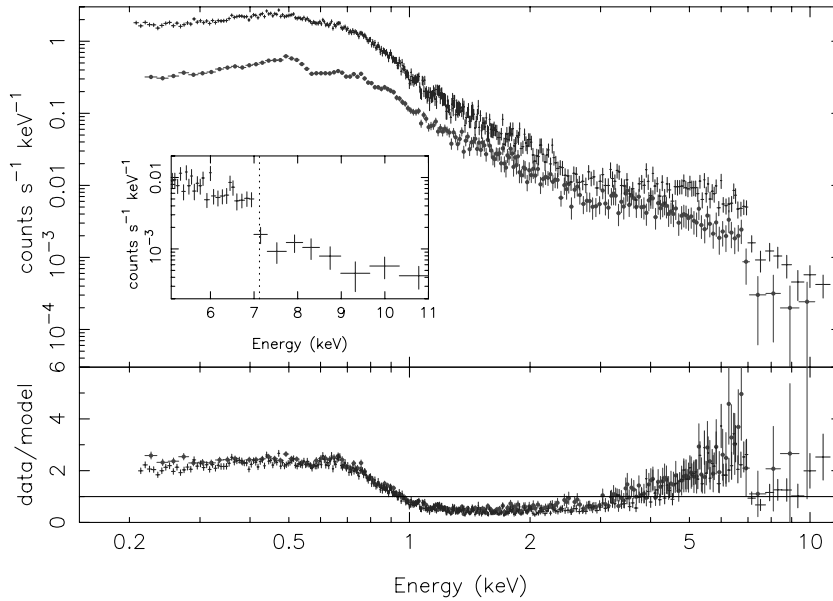


Figure 1. Raw EPIC pn (pluses) and MOS (filled circles) count spectra of 1H 0707 – 495 shifted to the rest frame of the source. (The MOS1 and MOS2 spectra were combined for display purposes only.) These spectra clearly show a significant drop at ~ 7 keV. The inset panel shows the pn spectrum, again in the rest frame of the source, with the expected position of the neutral iron K edge marked (dotted line). The bottom panel shows the data compared with a power-law model, with the slope fixed at $\Gamma = 2.7$. The model was not fitted to the data but chosen to emphasize the shape of the spectrum at both soft and hard energies.

L-shell absorption is unavoidable. The edge energy in the partial-covering model is 7.10 ± 0.04 keV, consistent with the energy of the neutral iron K edge. Fitting the 0.3–10 keV spectral energy distribution by adding a blackbody component does not affect the spectral parameters derived above.

3.3 Ionized reflection model

A strong Fe edge may be found in the reflected emission from an irradiated accretion disc that is not too highly ionized (Ross, Fabian & Young 1999). To investigate if such models can describe these data, the constant-density reflection models of Ross & Fabian (1993) were fitted to the 2–10 keV spectrum. Since the reflected emission may originate close to the central black hole, relativistic blurring was applied to the model during fitting (using the LAOR code: Laor 1991). Reflection from ionized material was strongly preferred over neutral reflection ($\Delta\chi^2 \approx -40$), an iron abundance approximately 3 times solar was needed ($\Delta\chi^2 = -10$ from a solar abundance model), and a Kerr space–time geometry was preferred over a Schwarzschild one ($r_{\text{in}} = 3\text{--}4$, $r_{\text{out}} = 8.3$ gravitational radii). However, a model with a reflection fraction of unity can only give an adequate fit to the data ($\chi^2 = 258/180$ dof) between 2 and 10 keV, and it cannot fully account for the sharp spectral drop at ~ 7 keV. Allowing the reflection fraction to increase to 9 resulted in a steeper continuum ($\Gamma = 1.68$ from 1.54) and an improved fit ($\chi^2 = 201/179$ dof; see Fig. 2). The high value of R can be decreased by increasing the iron abundance of the reflector. The ionization parameter is $\xi \approx 750$ erg cm s $^{-1}$. At this level of ionization the reflection-dominated model predicts a strong He-like Fe K α line with an equivalent width of 1.8 keV. This model clearly is not as good at describing the data as the partial-covering model. It is extremely difficult for ionized reflection to account for the depth of the drop at ~ 7 keV without invoking a very extreme Fe abundance and/or reflection fraction.

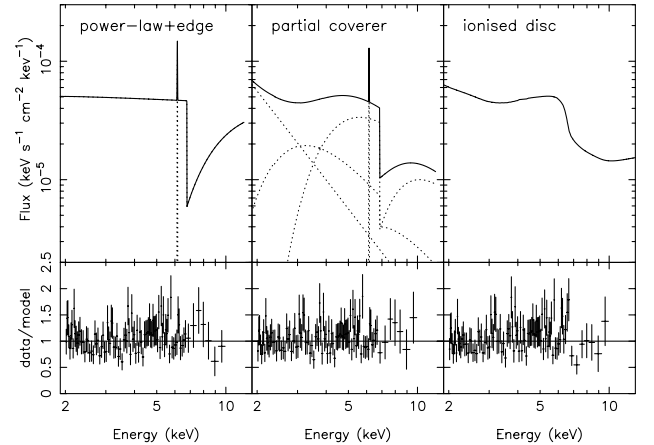


Figure 2. Spectral fits to the 2–10 keV EPIC data. The upper panels demonstrate the models (in F_x units) and the lower panels show the data/model residuals. The left-hand panels show the simple power-law and edge model, the middle panels show the partial-covering model, and the right-hand panels show the $3 \times$ solar Fe ionized reflection model.

3.4 Other models

The blue wing of a very strong relativistically broadened and highly redshifted iron K α line can produce a drop at 7 keV. A power-law plus LAOR line (rest energy 6.4 keV) provides a good fit ($\chi^2 = 182/180$ dof) with an inner disc radius $r_{\text{in}} < 2r_g$ and an underlying power-law slope of $\Gamma = 2.08^{+0.25}_{-0.13}$. However, the very high equivalent width ($EW = 5$ keV) required to explain the size of the 7-keV drop is difficult to justify. Alternatively, a reflection spectrum from cold material will contain a neutral iron edge. Fitting with a PEXRAV model gives a good fit ($\chi^2 = 192/182$ dof) with a reflection fraction ≥ 200 (essentially just reflection) and an iron overabundance > 3 . The dominance of the reflected compared with the primary emission and the weakness of the associated iron K α line appear fatal for this interpretation.

4 TEMPORAL ANALYSIS

Fig. 3 shows the 0.1–10 keV EPIC pn light curve in 200-s bins (The MOS light curves are essentially identical to the pn light curve.). The source again showed strong (factor of ~ 4 change during the observation) and rapid variability, as previously seen by ASCA (Leighly 1999a). The relatively low apparent luminosity of the source during this observation, $L_{0.2-10} \approx 8 \times 10^{42}$ erg s $^{-1}$, means that the rapid variability translates to a fairly modest rate of change of luminosity. For example, the rapid rise toward the end of the observation corresponds to a luminosity increase of $\Delta L/\Delta t \approx 2.4 \times 10^{39}$ erg s $^{-2}$. The corresponding radiative efficiency, using the argument of Fabian (1979), is only $\eta \gtrsim 0.2$ per cent.

Light curves in various energy bands were analysed to search for spectral variability. The variations in each band appear very similar. The fractional variability amplitude F_{var} (see Edelson et al. 2001) was measured in different energy bands (Fig. 4) using light curves binned to 1000 s, and is consistent with a constant (fractional) variability amplitude. A cross-correlation analysis using the discrete correlation function (DCF; Edelson & Krolik 1988) showed the light curves to be correlated at zero lag, with no evidence for any time lags.

Hardness ratios were also examined to search for spectral variability (see Fig. 5). These do show spectral variability (the lower two panels) but are uncorrelated with flux. As a final check of (flux-correlated) spectral variability, separate pn spectra were extracted from time intervals when the source flux was below the mean (‘low flux’ spectrum) and above the mean (‘high flux’ spectrum). The ratio of the two spectra (Fig. 6) is consistent with a constant, re-enforcing the claim of no flux-dependent spectral variability. Unfortunately, the limited number of counts above 7 keV (≈ 140 source counts in the pn) mitigates against a detailed analysis of the variability of the 7-keV spectral feature.

5 DISCUSSION

The *XMM-Newton* spectrum of 1H 0707 – 495 has revealed a sharp drop, by a factor $\gtrsim 2$, in the spectrum at an energy just above 7 keV. This is to our knowledge the first detection of such a feature in an AGN. The limited statistics and complex continuum mean that the identification of this feature remains ambiguous. We have considered models involving either partial covering of the X-ray source by cold material, or emission from an ionized accretion disc, but both these explanations have drawbacks.

5.1 Comparison of the two models

The energy of the feature is strongly suggestive of absorption by neutral iron. However, a complex partial-covering model is required in order that the soft X-ray spectrum be relatively unaffected by the absorber. A further implication of the partial-covering model is that the underlying power law is unusually steep ($\Gamma \approx 3.5$). A similar feature, namely a sharp drop near 7.1 keV with relatively little fluorescence emission, was observed in the peculiar X-ray binary Cir X-1 (Brandt et al. 1996). In this case the spectral feature is almost certainly due to partial covering.

An important consequence of the partial-covering model is that the unabsorbed X-ray luminosity of 1H 0707 – 495 is an order of magnitude higher than the observed (absorbed) luminosity. We have calculated the α_{ox} values for the absorbed and unabsorbed fluxes at 2 keV (the flux density at 2500Å is taken from Leighly 2000). The values are $\alpha_{\text{ox}} = -2.0$ (absorbed X-ray flux) and $\alpha_{\text{ox}} = -1.6$ (unabsorbed). This is suggestive of absorption (see Brandt,

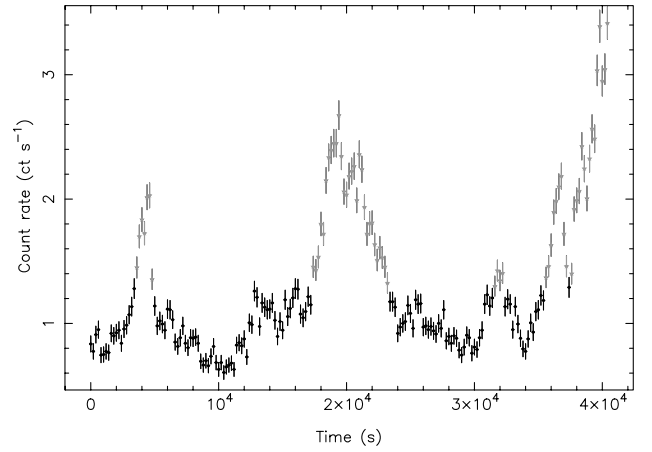


Figure 3. EPIC pn light curve in the 0.1–10 keV energy range with a bin size of 200 s, demonstrating the strong and rapid variability. The ‘high flux’ and ‘low flux’ intervals (see Section 4) are marked differently.

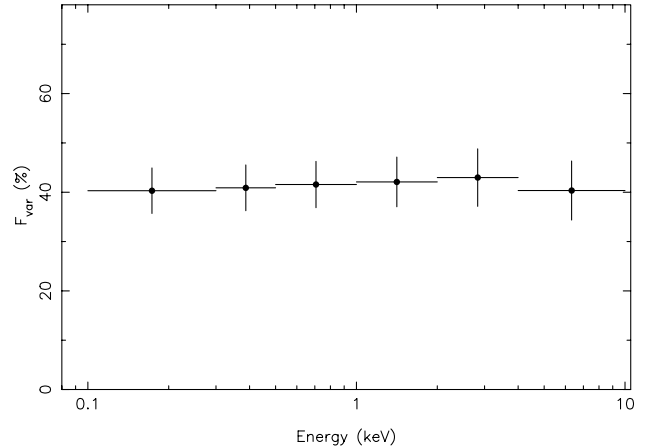


Figure 4. A plot of rms variability versus energy for the EPIC pn light curve.

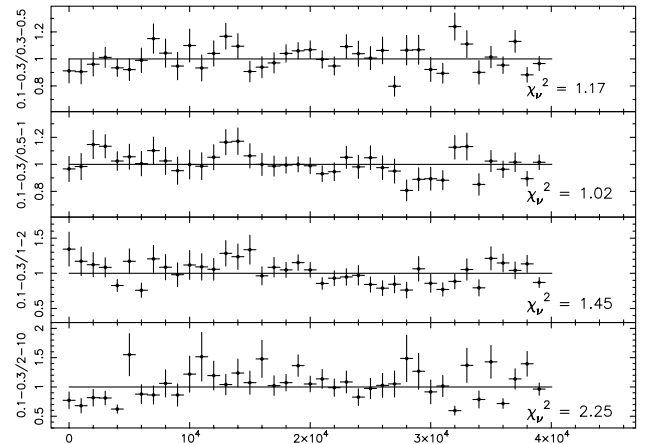


Figure 5. Hardness ratios using 1000-s time bins. The first two hardness ratios (at the top) are acceptable fits to a constant. The third is unacceptable at a ~ 95 per cent level; the last one is unacceptable at >99.9 per cent.

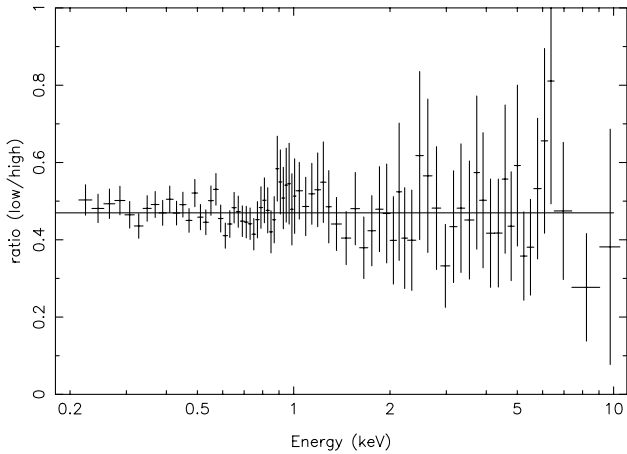


Figure 6. Ratio of ‘low flux’ and ‘high flux’ spectra.

Laor & Wills 2000; Brandt et al. 2001, fig. 3), as almost all the objects with $\alpha_{\text{ox}} < -1.8$ suffer from heavy UV and X-ray absorption. However, there is no evidence for intrinsic absorption in the *HST-STIS* spectrum of 1H 0707 – 495 (Leighly 2000).

The ionized disc model including relativistic blurring seems to provide another possibility for the sharp spectral feature. The blue horn of the relativistically broadened $K\alpha$ line emission, combined with the iron edge, can produce a drop around 7 keV. However, there still remain some residuals above 6.8 keV in the observer’s frame, and it appears somewhat surprising that the energy of the feature is almost exactly that of the neutral iron edge.

5.2 A physical scenario for the partial-covering model

The simplest configuration for the absorber would involve the absorber completely covering our line of sight, the unabsorbed flux being a scattered component from some other direction. This scattered component would not then vary rapidly and so would cause spectral variability when combined with the (variable) absorbed flux. If on the other hand the absorber does partially cover the source then it presumably is at most only a few hundred light-seconds in size and its density exceeds $\sim 10^{12} \text{ cm}^{-3}$. Photoionization considerations require that the cloud thickness be less than $\sim 10^{12} r_{15}^2 \text{ cm}$, where the distance of a cloud from the nucleus is $r_{15} 10^{15} \text{ cm}$. The source position, size and spectrum must remain fixed while the flux is rapidly varying in order to avoid strong spectral variability.

These problems are alleviated if the absorbers are close to, or even within, the emission region. The absorbing clouds must then be very dense to remain cool and therefore held by magnetic fields. The possible presence of such clouds in AGN in general has been discussed by Rees (1987), Celotti, Fabian & Rees (1992), Kuncic, Blackman & Rees (1996), Kuncic, Celotti & Rees (1997) and Malzac (2001). Brandt & Gallagher (2000) first suggested that such clouds might be particularly relevant for NLS1s. Cool gas trapped by the magnetic field is compressed to extreme densities by the high radiation pressure. Clouds and filaments of such cold gas may accompany the active regions above an accretion disc.

This possibility has been investigated using a relativistically blurred model involving emission and partial covering. In order that the 7.1-keV feature remains sharp in the model, the inclination must be $\lesssim 15^\circ$. If the absorbing material lies outside the emission region (say, in a toroidal structure at 10^{15} cm) then only the line-of-sight material affects the spectrum and this constraint is relaxed.

It is interesting to speculate whether the absorbing material is connected with the radiation-driven outflow suggested by Leighly (2000) in 1H 0707 – 495, and whether it affects the observed rapid X-ray variability. Clearly it is crucial to search for similar features in other objects. The *XMM-Newton* spectrum of PG 1211 + 143 (Reeves et al., in preparation) appears to show a similar drop at $\sim 7.3 \text{ keV}$. If such features are common in other objects, this will further constrain the range of suitable models.

ACKNOWLEDGMENTS

This Letter is based on observations obtained with *XMM-Newton*, an ESA science mission with instruments and contributions directly funded by ESA Member States and the USA (NASA). WNB acknowledges the financial support of NASA grant NAG5-9939. We thank Gareth Griffiths and Michael Freyberg for advice about the EPIC calibration, and the anonymous referee for constructive comments.

REFERENCES

- Arnaud K., 1996, in Jacoby G., Barnes J., eds, ASP Conf. Ser. Vol. 101, Astronomical Data Analysis Software and Systems. Astron. Soc. Pac., San Francisco, p. 17
- Bambynek W. et al., 1972, *Rev. Mod. Phys.*, 44, 716
- Bearden J. A., 1964, X-ray wavelengths. US Atomic Energy Commission, Tennessee, USA
- Boller Th., Brandt W. N., Fink H., 1996, *A&A*, 305, 53
- Brandt W. N., Boller Th., 1998, *Astron. Nachr.*, 319, 163
- Brandt W. N., Gallagher S. C., 2000, *New Astron. Rev.*, 44, 461
- Brandt W. N., Fabian A. C., Dotani T., Nagase F., Inoue H., Kotani T., Segawa Y., 1996, *MNRAS*, 293, 1071
- Brandt W. N., Laor A., Wills B. J., 2000, *ApJ*, 528, 637
- Brandt W. N., Guainazzi M., Kaspi S., Fan X., Schneider D. P., Strauss M. A., Clavel J., Gunn J. E., 2001, *AJ*, 121, 591
- Celotti A., Fabian A. C., Rees M. J., 1992, *MNRAS*, 255, 419
- Dickey J. M., Lockman F. J., 1990, *ARA&A*, 28, 215
- Edelson R., Krolik J. H., 1988, *ApJ*, 333, 656
- Edelson R., Griffith G., Markowitz A., Sembay S., Turner M. J. L., Warwick R., 2001, *ApJ*, submitted
- Fabian A. C., 1979, *Proc. R. Soc. London, Ser. A*, 366, 449
- Henke B. L., Gullikson E. M., Davis J. C., 1993, *Astron. Data Nucl. Data Tables*, 54, 181
- Holt S. S., Mushotzky R. F., Boldt E. A., Serlemitsos P. J., Becker R. H., Szymkowiak A. E., White N. E., 1980, *ApJ*, 241, L13
- Kuncic Z., Blackman E. G., Rees M. J., 1996, *MNRAS*, 283, 1322
- Kuncic Z., Celotti A., Rees M. J., 1997, *MNRAS*, 284, 717
- Laor A., 1991, *ApJ*, 376, 90
- Leighly K. M., 1999a, *ApJS*, 125, 279
- Leighly K. M., 1999b, *ApJS*, 125, 317
- Leighly K. M., 2000, *New Astron. Rev.*, 44, 395
- Malzac J., 2001, *MNRAS*, 325, 1625
- Pounds K. A., Done C., Osborne J. P., 1995, *MNRAS*, 277, L5
- Rees M. J., 1987, *MNRAS*, 228, 47
- Remillard R. A., Bradt H. V., Buckley D. A., Roberts W., Schwartz D. A., Tuohy I. R., Wood K., 1986, *ApJ*, 301, 742
- Ross R. R., Fabian A. C., 1993, *MNRAS*, 261, 74
- Ross R. R., Fabian A. C., Young A. J., 1999, *MNRAS*, 306, 461
- Strüder L., Briel U., Dennerl K., Hartmann R., Kendziorra E., Meidinger N., Pfefferman E., Reppin C., 2001, *A&A*, 365, L18
- Turner T. J., George I. M., Nandra K., Turcan D., 1999, *ApJ*, 524, 667
- Vaughan S., Reeves J., Warwick R., Edelson R., 1999, *MNRAS*, 309, 113
- Vaughan S., Edelson R., Warwick R. S., Malkan M. A., Goad M. R., 2001, *MNRAS*, 327, 673

This paper has been typeset from a $\text{\TeX}/\text{\LaTeX}$ prepared by the author.